Available online at www.sciencedirect.com
ScienceDirect
International Journal of Thermal Sciences 46 (2007) 128–138
International Journal of Thermal Sciences
www.elsevier.com/locate/ijts

Estimation of the parameters of a Gaussian heat source by the Levenberg–Marquardt method: Application to the electron beam welding

S. Rouquette, J. Guo, P. Le Masson *

LET2E: Laboratoire d'Etudes Thermiques Energétique et Environnement, Université de Bretagne Sud, Centre de recherche, rue de saint Maudé, F-56321 Lorient cedex, France

Received 15 April 2005; received in revised form 20 January 2006; accepted 12 April 2006

Available online 30 June 2006

Abstract

In this paper, we estimate a heat source in a longitudinal section during an electron beam welding. The aim of this work is the parameter identification of the Gaussian source term representative of the dissipated heat flux in the liquid zone from measured temperatures in the solid zone. In a previous work [J. Guo, P. Le Masson, E. Artioukhine, T. Loulou, P. Rogeon, M. Carin, M. Dumons, J. Costa, Estimation of a source term in a two-dimensional heat transfer problem: Application to an electron beam welding, in: 4th Int. Conf. Inverse Problems, Russia, 2003], we have analyzed the feasibility of the estimation for a source term $S(x, z, t)$ in a transversal section. This work has an application in the electron beam welding of steels of thickness about 8 cm. The direct thermo-metallurgical problem is presented in a two-dimensional longitudinal section (x, y) for a quasi-steady state. This non-linear problem is considered in the thesis of J. Guo [J. Guo, Estimation de la distribution énergétique induite par un faisceau d'électrons dans un matériau métallique – Application au cas du soudage d'un acier, Thèse de l'université de Bretagne Sud, 2005]. Here, we solve only a linear case. The sample is divided in the axial direction z in few sections. At each section, a source term is defined with a part of the beam and creates a vaporized zone and a fused zone. The goal of this work is the rebuilding of the complete source term with the estimations at each section. In this paper, the feasibility of the parameter estimation by Levenberg–Marquardt method is analyzed.

Keywords: Levenberg–Marquardt method; Inverse problem; Electron beam welding

1. Introduction

Welding is an assembling operation which affects both mechanical and metallurgical properties and which is very sensitive to the control parameters of the technological processes. The first stage of this study is to choose parameters which lead to an acceptable welding quality. The main difficulty of the theoretical analysis is that the exact distribution of the thermal energy absorbed and generated in the liquid and vapor zones is not easy to predict and cannot be measured directly. When studying the welding, the theoretical analysis uses complementary experimental informations: the temperature measurements near the liquid zone and the microstructural properties (hardness, optical micrography, etc.).

The objective of this work is the estimation of the energy distribution in the welding zone. The problem is that there is a strong damping effect in the solid zone. The reason of this effect is related to a great difference in temperature between the weld bead and the base metal. That is why it is difficult to estimate correctly the energy distribution from the temperature measurements located at points which are too far from the welding zone.

Many works deal with the estimation of boundary conditions or the determination of the heat flux distribution on the boundary of the workpiece [2–4]. Few of these works consider experimental situations involving unknown heat sources. Silva Neto et al. [5] used the conjugate gradient algorithm to estimate the time-varying strength of a line source placed in a rectangular region with insulated boundaries, but the location of the source was specified. Le Niliot [6] studied linear inverse prob-

* Corresponding author.
E-mail addresses: sebastien.rouquette@utt.fr (S. Rouquette), jialin.guo@univ-ubs.fr (J. Guo), philippe.le-masson@univ-ubs.fr (P. Le Masson).

1290-0729/$ – see front matter
doi:10.1016/j.ijthermalsci.2006.04.015

Nomenclature

b	constant of the austenite–martensite transformation
C_p, C_γ, C_α	specific heat ..... $\mathrm{J\,kg^{-1}\,K^{-1}}$
$\partial T/\partial t$	variation of the temperature with time ..... $\mathrm{K\,s^{-1}}$
$f(\frac{\partial T}{\partial t}), f(\frac{\partial T}{\partial y})$	function of the cooling or warming speed
h	penetration ..... m
H, H_α, H_β	enthalpies ..... $\mathrm{J\,m^{-3}}$
$\Delta H_{\mathrm{fus}}, \Delta H_{\mathrm{vap}}$	enthalpies of the phase change ..... $\mathrm{J\,kg^{-1}}$
I_b, I_f	current and focus current ..... A
$J_{P_W}, J_{W_{FE}}, J_{y_s}$	sensitivity coefficients
$J(P)$	sensitivity matrix
$L_{\alpha\gamma}$	heat transformation of phase α to γ ..... $\mathrm{J\,m^{-3}}$
M_s	martensite start temperature
P_W, P_W^0, P_W^k	power of the source ..... $\mathrm{W\,m^{-1}}$
P, P_{eq}	proportion of metallurgic phase (per volume fraction)
$P_{\max}$	maximum proportion of the austenite phase during the austenite–martensite transformation
P_α, P_γ	proportion of the ferrite and austenite phase
$S(x,z,t), S(x,\xi,t), S(x,y)$	source term
$S(P)$	residual functional
T_{inf}	external temperature ..... °C
T, T_0	temperature in the sample and initial temperature in the sample ..... °C
t	time coordinate ..... s
U	voltage V
V	velocity ..... $\mathrm{m\,s^{-1}}$
$W_{FE}, W_{FE}^0, W_{FE}^k$	parameter of the Gaussian source
x, y, z, ξ	spatial coordinates ..... m
$X_{P_W}, X_{W_{FE}}, X_{y_s}$	normalized sensitivity coefficients
Y, Y_i, Y_e	experimental temperatures ..... °C
y_s, y_s^0, y_s^k	source position ..... m
ε'	coefficient
ε	emissivity of the sample
$\varepsilon_{\mathrm{stop}}$	arrest criterion
η	efficiency coefficient
$\lambda, \lambda_\alpha, \lambda_\gamma$	conductivity ..... $\mathrm{W\,m^{-1}\,K^{-1}}$
λ^0, λ^k	damping parameter
$\rho, \rho_\alpha, \rho_\gamma$	density ..... $\mathrm{kg\,m^{-3}}$
σ	Boltzmann constant: $5.67 \times 10^{-8}\ \mathrm{W\,m^{-2}\,K^{-4}}$
τ	Time constant
Φ_E	beam diameter ..... m
Ω^k	diagonal matrix

lems with two point heat sources, and experimental results were presented in [7].

In many studies, the inverse fusion and solidification problem have been analyzed with a simplified approach only based on a conduction model in the liquid and vapor zones. Under these assumptions, 1D or 2D Stefan problems taking into account only the conduction effects in all the phases during the process were considered. The objective was to estimate an energy distribution [4], or a motion of the solid–liquid interface [8–11]. Another approach which takes into account the convection effects described by the Navier–Stokes equations in the liquid and vapor zones, was used in [12]. Finally, mixed approaches in which an apparent source term is determined in the liquid and vapor zones representing the different phenomena, were utilized in [13].

In this paper, we use the first assumption for the electron beam welding process. We consider only the conduction effects for all phases (solid, liquid and vapor). The Levenberg–Marquardt method [14,15] is used to estimate the parameters of the dissipation energy in the liquid and vapor zones. First, we present the electron beam welding technique and the used steel sample. Second, the direct problem is described with the description of the Gaussian heat source distribution. Third, sensitivity analysis is investigated for each parameter which we want to estimate. Fourth, the estimation procedure is described and numerical cases are studied. At last, the estimation results are discussed for experimental and numerical data.

2. The electron beam welding process

The electron beam (EB) welding is an assembling process in vacuum using a high density energy beam. This technology allows the welding of the high thicknesses (up to 16 cm) with a low width and a narrow Heat Affected Zone (HAZ). At the beginning of the welding process, the high power density of the electron beam leads to an evaporation of the material and then to a keyhole (Fig. 1). It is this moving keyhole which generates the welded joint. The high penetration capacity of the beam with a narrow fusion zone characterizes the electron beam welding in comparison with other welding technologies. For these other methods, the penetration is limited by the heat conduction [16].

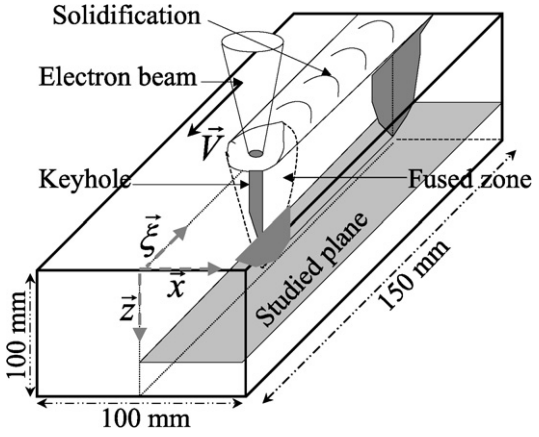

Fig. 1. Welding process and studied domain.

The weld joints are realized at the DCN-propulsion (power of this electron beam: 100 kW). The workpieces are made with 18MnNiMo 5 steel plates (equivalent to ASTM A508 Cl.3 in USA). In our study, a partial penetration welded joint is analyzed. Fig. 2 shows the micrography of this sample which is

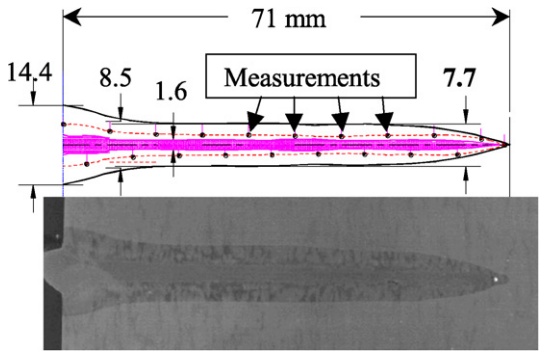

Fig. 2. Weld Joint (dimensions in mm).

used to determine precisely the locations of the measurement points by using a macrography of this welding joint. The welding parameters are: voltage: $U = 60$ kV, current $I_b = 0.29$ A, velocity $V = 2.5\ \mathrm{mm\,s^{-1}}$, focus current $I_f = 2.46$ A, etc. The paper of Carin et al. [17] presents an example of the experimental parts.

The high temperature level in the fusion and vapor zones does not permit the installation of the thermocouples in these zones. The used thermocouples ($d = 50$ or 80 μm; K type, C type or S type) are thus located in the HAZ ($750\,^\circ\mathrm{C} < T < 1450\,^\circ\mathrm{C}$).

3. The direct heat conduction problem

3.1. Equations of the direct problem

Several works are concerned with the numerical simulation of the EB welding in our laboratory [17,18,21]. In these works, the commercial code SYSWELD [19] and a new code analogous to SYSWELD which is incorporated in the optimization code developed were used. The studied domain is one half of the longitudinal section taken perpendicularly to the beam axis (Fig. 1). In a transient description, the equations are the heat conduction equation (1) and the metallurgical kinetic equations (2) of the Leblond and Devaux and Koistinen and Marburger type [1]

$$C(T)\frac{\partial T}{\partial t} = \frac{\partial}{\partial x}\left(\lambda(T)\frac{\partial T}{\partial x}\right) + \frac{\partial}{\partial \xi}\left(\lambda(T)\frac{\partial T}{\partial \xi}\right) + \frac{\mathrm{d}P_\alpha}{\mathrm{d}t}L_{\alpha\gamma}(T) - \frac{\partial(\rho H)}{\partial t} + S(x,\xi,t) \tag{1}$$

$$\frac{\mathrm{d}P}{\mathrm{d}t} = \frac{P_{\mathrm{eq}} - P}{\tau} f\left(\frac{\mathrm{d}T}{\mathrm{d}t}\right) \quad \text{and}$$
$$P = P_{\max}\big(1 - \exp\big(-b(T - M_s)\big)\big) \tag{2}$$

In Eq. (1), the thermophysical characteristics $C(T) = c(T)\rho(T)$ and $\lambda(T)$ are calculated by a law of mixture according to the temperatures.

$$C(T) = P_\alpha c_\alpha(T)\rho_\alpha(T) + P_\beta c_\beta(T)\rho_\beta(T)$$

and

$$\lambda(T) = P_\alpha \lambda_\alpha(T) + P_\beta \lambda_\beta(T)$$

with P_α and P_β the proportional phases obtained from Eq. (2). A Continuous Cooling Temperature (C.C.T.) diagram is used for the definition of the parameters in Eq. (2). At each node of the grid, the temperature and the cooling speed or the heating speed are used to obtain the proportion of phases. In the heat conduction equation (1), the source terms $\frac{\mathrm{d}P_\alpha}{\mathrm{d}t}L_{\alpha\gamma}(T)$ and $\frac{\partial(\rho H)}{\partial t}$ allow to take into account the phase change enthalpy according to the temperature of the sample (metallurgical transformations for the first term P_α is the proportion of metallurgic phase α, fusion and evaporation for the second). The transformation energy is calculated according to the phase enthalpy: $L_{\alpha\gamma}(T) = \rho_\gamma H_\gamma - \rho_\alpha H_\alpha$ and by considering two metallurgical phases only: γ (austenite) and α (ferrite, perlite, bainite or martensite). The enthalpies of the phases α and γ are computed with the use of polynomial functions between 100 °C and 1450 °C. The other thermal transformations are computed between 1450 °C and 1550 °C for the fusion and between 2600 °C and 2800 °C for the evaporation. These enthalpies are given in Costantini work [16]: $\Delta H_{\mathrm{fus}} = 391970\ \mathrm{J\,kg^{-1}}$ and $\Delta H_{\mathrm{vap}} = 6332879\ \mathrm{J\,kg^{-1}}$. At last, the thermophysical characteristics of the liquid and vapor phases are computed at the temperature 1450 °C.

The boundary and initial conditions are the following: at the lateral surfaces, only the radiative conditions are fixed because the welding process is carried out in vacuum. For example at the lateral surface in $x = x_{\max}$, the boundary condition is:

$$-\lambda(T)\frac{\partial T(x_{\max},\xi,t)}{\partial x} = \varepsilon\sigma\left[T^4(x_{\max},\xi,t) - T_{\mathrm{inf}}^4\right] \tag{3}$$

On the axis:

$$\frac{\partial T(x=0,\xi,t)}{\partial x} = 0 \tag{4}$$

Initial conditions:

$$T(x,y,0) = T_0; \qquad P_\alpha(x,y,0) = 1 \tag{5}$$

For this study, we use a quasi stationary problem and we define a moving coordinate system (x, y), where $y = \xi + Vt$. In the stationary regime ($\frac{\partial T}{\partial t} = 0$), the heat conduction equation and the metallurgical kinetic equations become (6) and (7):

$$VC(T)\frac{\partial T}{\partial y} = \frac{\partial}{\partial x}\left(\lambda(T)\frac{\partial T}{\partial x}\right) + \frac{\partial}{\partial y}\left(\lambda(T)\frac{\partial T}{\partial y}\right) + V\frac{\mathrm{d}P_\alpha}{\mathrm{d}y}L_{\alpha\gamma}(T) - V\frac{\partial(\rho H)}{\partial y} + S(x,y) \tag{6}$$

$$V\frac{\mathrm{d}P}{\mathrm{d}y} = \frac{P_{\mathrm{eq}} - P}{\tau} f\left(\frac{\mathrm{d}T}{\mathrm{d}y}\right) \quad \text{and}$$
$$P = P_{\max}\big(1 - \exp\big(-b(T - M_s)\big)\big) \tag{7}$$

For this new problem, we take only a part of the longitudinal section. The boundary conditions in the beam direction "y" change and we set these new conditions:

$$\text{at } y = y_{\min} \quad T = T_0 \tag{8}$$

$$\text{at } y = y_{\max} \quad \frac{\partial T}{\partial y} = 0 \tag{9}$$

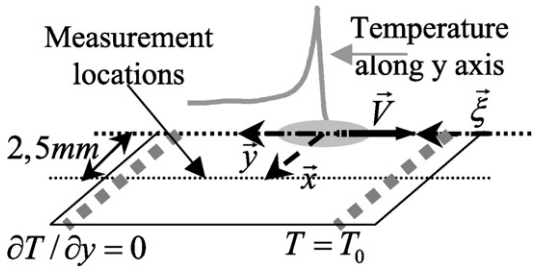

Fig. 3. Studied section and measurement locations.

For the conditions in the transverse direction "x", we have the same boundary conditions. Fig. 3 shows the study section with the new conditions.

In Eq. (6), the term $S(x, y)$ is the source term which represents the energy of the electron beam. The Gaussian source term corresponds to several studies carried out in our laboratory [18]:

$$S(x,y) = f(z_e) * \frac{8\eta U I_b}{\pi \Phi_E^2} \exp\left(-\frac{8(x^2+(y-y_S)^2)}{\Phi_E^2}\right)$$
$$\text{with } f(z_e) = \frac{2}{h}\left(1-\frac{z_e}{h}\right) \tag{10}$$

where the parameters are: efficiency coefficient $\eta = 0.9$, voltage: $U = 60$ kV, current: $I_b = 0.29$ A, velocity: $V = 2.5\ \mathrm{mm\,s^{-1}}$, penetration: $h = 71$ mm, beam diameter: $\phi_E = 1$ mm and z_e: the depth of the longitudinal section.

The goal of this study is the estimation of the parameters describing the source term by the Levenberg–Marquardt method. So, first, the source term which has been presented above is defined mainly by three parameters (P_W, W_{FE}, y_S):

$$S(x,y) = \frac{P_W}{W_{FE}^2} \exp\left(-\left(\frac{x^2+(y-y_S)^2}{W_{FE}^2}\right)\right) \tag{11}$$

where P_W is the power of the electron beam, W_{FE}, equal to $\sqrt{\phi_E^2/8}$, is the parameter of the Gaussian source and y_S is the position of the source in this quasi-steady problem. Second, we analyze only a linear problem without metallurgical transformations and with constants thermophysical characteristics.

3.2. Numerical resolution of the direct problem

To solve the direct problem, we need to define the value of the parameters of the model. So, the thermophysical parameters are taken constant: $\rho = 7500\ \mathrm{kg\,m^{-3}}$, $C_p = 520\ \mathrm{J\,kg^{-1}\,K^{-1}}$, $\lambda = 32\ \mathrm{W\,K^{-1}\,m^{-1}}$ and $\varepsilon = 0.8$. The parameters values of the Gaussian source are estimated as following:

- $P_W = \frac{2}{h}\left(1-\frac{z_e}{h}\right)\left(\frac{\eta U I}{\pi}\right)$ with $z_e = 0.041$ m, $h = 0.071$ m, $\eta = 0.9$, $U = 60$ kV and $I_b = 0.29$ A lead to $P_W \approx 60\ \mathrm{kW\,m^{-1}}$;
- $y_S = 0.015$ m;
- $W_{FE} = \sqrt{\phi_E^2/8}$ with $\phi_E = 1$ mm the experimental beam diameter gives $W_{FE} = 3.53 \times 10^{-4}$ m.

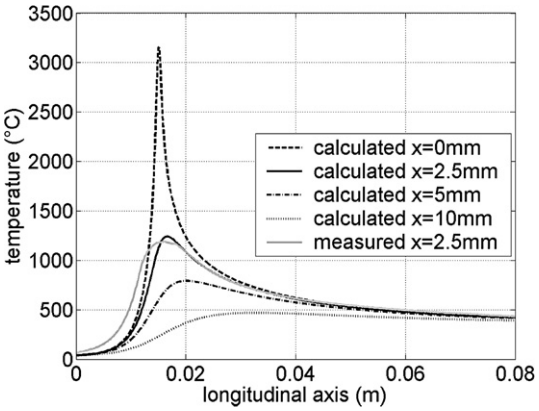

Fig. 4. Comparison between measured and calculated temperatures.

The spatial domain is defined as: $y_{\min} = 0$ m, $y_{\max} = 0.08$ m, $x_{\min} = 0$ m and $x_{\max} = 0.03$ m. The choice of these values has been validated in the paper of Rogeon et al. [17] in the transverse direction ($O\vec{x}$) where in the linear case, effects due to the boundary domain are insignificant above $x \geqslant 20$ mm. In the longitudinal direction ($O\vec{y}$), the experimental and calculated kinetics tend to horizontal ($\partial T/\partial y = 0$) for $y \geqslant 80$ mm. The meshgrid of the domain is defined by 4133 nodes and the number of triangular elements is 7862. The minimum area is 4.73×10^{-10} m^2 near the source and the maximum area is 3.58×10^{-6} m^2 for elements far away from the source. A quadratic Lagrangian finite element are used in this mesh. An iterative method is employed to solve the problem by using the Good Broyden Solver with the incomplete LU preconditioner. These results are computed using Femlab 2.3 finite element code. Fig. 4 presents the calculated temperature at four different positions: $x = 0$ mm, 2.5 mm, 5 mm and 10 mm and a comparison between measured temperature at $x = 2.5$ mm.

At $x = 2.5$ mm, the maximum temperature calculated is inferior to the temperature of melted steel ($T_f \sim 1450\,^\circ$C). For the experimental conditions, the temperature acquisition seems to be difficult in the melted zone. In this study, the thermocouple K is employed due to their sensitivity and their measurement scale which is limited punctually at a maximum temperature of 1300 °C. That is why, measurements are possible in the Heat Affected Zone (HAZ) at abscissa $x = 2.5$ mm (experimentally measurements are taken between $x = 2$ mm and $x = 3$ mm).

In Fig. 4, at $x = 2.5$ mm, some differences between the calculated and measured temperatures at the same abscissa are observed. The experimental temperature evolution is larger, the position of the source seems to be different but the power is quite the same with similar maximum temperatures. The experimental and calculated thermal cycles are similar during the cooling phase for $y \geqslant 20$ mm. These differences are related to the thermophysical characteristics which are assumed constants.

So, for the estimation of the unknown parameters: P_W, W_{FE} and y_S, we have developed an inverse approach.

4. The inverse problem of the parameter estimation

4.1. The Levenberg–Marquardt method

The inverse problem consists in the minimization of a quadratic functional (or cost function) $S(P)$ where $P = \{P_W, W_{FE}, y_S\}$ is the set of unknown parameters. The solution of the inverse problem is obtained when the minimization of the difference between the calculated and measured temperatures (in the sense of the least square method) is realized.

The expression of this quadratic functional is:

$$S(P) = [Y_i - T_i]^{\mathrm{T}}[Y_i - T_i] \tag{12}$$

where Y_i are the measured temperatures and T_i the calculated temperatures taken at abscissa $x = 2.5$ mm from the line source position (Fig. 4). $i = 1, \ldots, I$ is the number of the measurement points: $[Y_i - T_i]^{\mathrm{T}} = [Y_1 - T_1, Y_2 - T_2, \ldots, Y_I - T_I]$. The subscript $^{\mathrm{T}}$ denotes the transpose.

The method used to solve this inverse problem is the Levenberg–Marquardt method. This method is useful when the number of the parameters to identify is low (typically less than 5 ...). This technique is an iterative method for solving nonlinear least squares problems of the parameter estimation [20]. The Levenberg–Marquardt method has been applied to the solution of a variety of inverse problem involving the estimation of unknown parameters [14,15,20].

The Levenberg Marquardt method consist in correcting the unknown set of parameters by the following formula:

$$P^{k+1} = P^k + \left[\left(J^k\right)^{\mathrm{T}} W J^k + \lambda^k \Omega^k\right]^{-1} \times \left[\left(J^k\right)^{\mathrm{T}} W (T_i - Y_i)\right] \tag{13}$$

where λ^k is a positive scalar named damping parameter and Ω^k is a diagonal matrix. The goal of the term $\lambda^k \Omega^k$ is to damp the oscillations and instabilities due to the ill-conditioned character of the problem. This damping parameter is large at the beginning of the iterative procedure (and the method is like the steepest descent method) then it decreases when the procedure advances to the solution (and the method tends to the Gauss method). W is a diagonal matrix where the diagonal elements are given by the inverse of the standard deviation of the measurement errors. The sensitivity matrix $J(P)$ is written as:

$$J(P) = \begin{bmatrix} \frac{\partial T_1}{\partial P_W} & \frac{\partial T_1}{\partial W_{FE}} & \frac{\partial T_1}{\partial y_S} \\ \frac{\partial T_2}{\partial P_W} & \frac{\partial T_2}{\partial W_{FE}} & \frac{\partial T_2}{\partial y_S} \\ \cdots & \cdots & \cdots \\ \frac{\partial T_I}{\partial P_W} & \frac{\partial T_I}{\partial W_{FE}} & \frac{\partial T_I}{\partial y_S} \end{bmatrix} \tag{14}$$

where I is the total number of measurements. The elements of the sensitivity matrix are called the sensitivity coefficients. The sensitivity coefficient J_{ij} is thus defined as the first derivative of the calculated temperature at position y_i with respect to the unknown parameter P_j, $P_j \in P = \{P_W, W_{FE}, y_S\}$: $J_{ij} = \partial T_i / \partial P_j$.

The success of this estimation procedure is associated with the choice of λ^k and the information contained in the sensitivity matrix. The sensitivity matrix plays a fundamental role in the parameter estimation. In fact, when the sensitivity coefficients are small, we have $|J^{\mathrm{T}} J| \approx 0$ and the inverse problem is ill-conditioned. It can also be shown that $|J^{\mathrm{T}} J|$ is null if any column of $J(P)$ can be expressed as a linear combination of the other columns. Therefore, it is desirable to have linearly-independent sensitivity coefficients J_{ij} with large magnitudes. In that case, the inverse problem is not very sensitive to measurement errors and accurate estimates of the parameters can be obtained.

In problems involving parameters with different orders of magnitude, the sensitivity coefficients with respect to the various parameters may also differ by several orders of magnitude, creating difficulties in their comparison and identification of linear dependence. These difficulties can be alleviated through the analysis of their dimensionless sensitivity coefficients or normalized sensitivity coefficients defined here as:

$$X_{P_W} = P_W \frac{\partial T}{\partial P_W} \qquad X_{W_{FE}} = W_{FE} \frac{\partial T}{\partial W_{FE}}$$
$$X_{y_S} = y_S \frac{\partial T}{\partial y_S} \tag{15}$$

These normalized sensitivity coefficients have the units of the temperature; hence, their effect on the temperature field is easier to analyze.

4.2. Sensitivity coefficients calculus

For the sensitivity coefficients calculus, we have three methods [20]. Here, a central difference method is used to estimate the sensitivity coefficients, for example:

$$J_i(P_W) = \frac{T_i(P_W + \varepsilon' P_W, W_{FE}, y_S) - T_i(P_W - \varepsilon' P_W, W_{FE}, y_S)}{2\varepsilon' P_W} \tag{16}$$

where $T_i(P_W + \varepsilon' P_W, W_{FE}, y_S)$ and $T_i(P_W - \varepsilon' P_W, W_{FE}, y_S)$ are the calculated temperatures for the parameter P_W with a little variation $\varepsilon' P_W$. Few values of ε' have been investigated ($10^{-6} \leqslant \varepsilon' \leqslant 10^{-1}$) and our choice is $\varepsilon' = 0.005$.

The code Femlab is a multiphysic code which allows to solve coupled PDE's systems. So, we have defined seven systems: one for the direct problem and six for each perturbed problems ($P_W + \varepsilon' P_W$, $P_W - \varepsilon' P_W$, $W_{FE} + \varepsilon' W_{FE}$, $W_{FE} - \varepsilon' W_{FE}$, $y_S + \varepsilon' y_S$, $y_S - \varepsilon' y_S$). After the definition of these seven systems in femlab, we save this definition in a matlab file (*.m). Then, an optimization algorithm has been implemented in this file.

4.3. Parameter sensitivity analysis

The distribution of normalized sensitivity coefficients computed are plotted in Figs. 5–7.

First, we remark that the evolution of the normalized sensitivity coefficients P_W (Fig. 5) are similar to the temperature evolution (Fig. 4). In fact, due to our linear hypothesis when the normalized sensitivity coefficients are calculated, we obtained the temperature field. The sensitivity coefficient P_W can

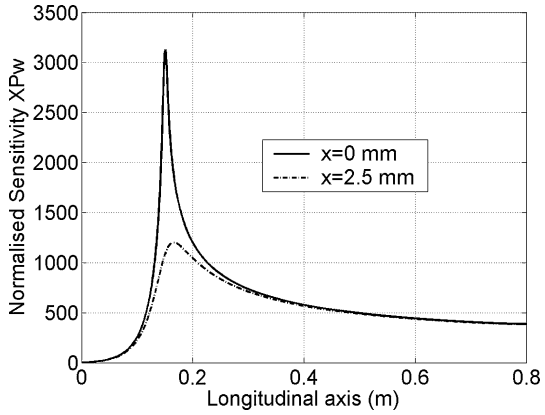

Fig. 5. Normalized sensitivity coefficient for P_W.

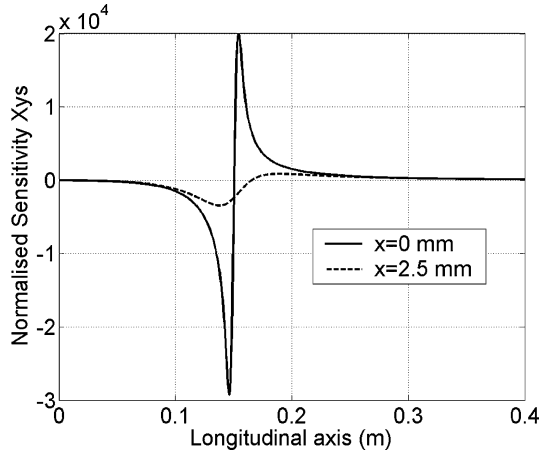

Fig. 6. Normalized sensitivity coefficients for y_S.

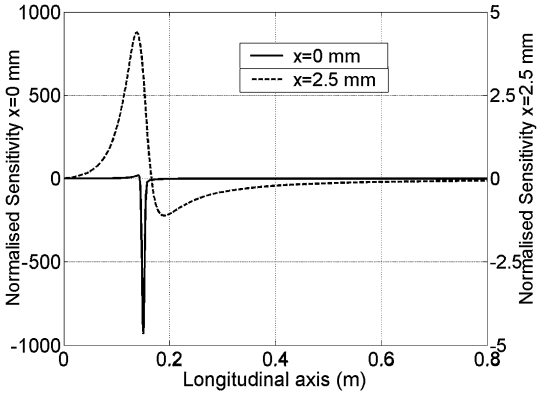

Fig. 7. Normalized sensitivity coefficient for W_{FE}.

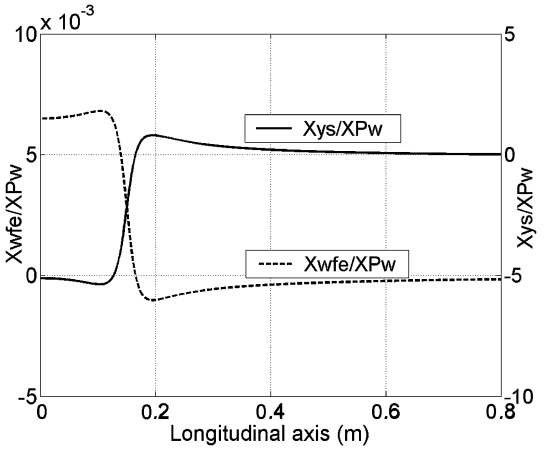

Fig. 8. Evolution of the ratios $X_{W_{FE}}/X_{P_W}$ and X_{y_S}/X_{P_W} at 2.5 mm from the source axis.

be computed by the derivation of the linear conduction equation by P_W: $J_{P_W} = \partial T/\partial P_W$. The main equation becomes:

$$C\frac{\partial J_{P_W}}{\partial t} = \lambda \Delta J_{P_W} + \frac{\partial S}{\partial P_W}$$

$$\text{where } \frac{\partial S}{\partial P_W} = \frac{1}{W_{FE}^2}\exp\left(-\left(\frac{x^2+(y-y_S)^2}{W_{FE}^2}\right)\right) \tag{17}$$

When the normalized sensitivity is calculated by multiplying J_{P_W} by P_W, this previous equation gives the heat conduction equation. So the normalized sensitivity coefficient field is similar to the temperature field.

We note the normalized sensitivity coefficient is twice less influent at $x = 2.5$ mm than at $x = 0$ mm. The maximum value of X_{P_W} at $x = 2.5$ mm is about 1200 °C. These values seem to be sufficient to perform the P_W identification because they are bigger than the measurement errors.

Second, for the y_S normalized sensitivity coefficient, the magnitude is large near the real value of y_S (Fig. 6). Before this position ($y \leqslant y_S$) the normalized sensitivity coefficients are negative and the maximum value is around −3500 °C. For values $y \geqslant y_S$ the maximum value is around 900 °C. So the estimation seems to be possible due to the magnitude of these coefficients. We note that this coefficient is proportional to $-\partial T/\partial y$ in $x = 2.5$ mm (at $y \approx 0.0166$ m, we have $T_{\max}$ and $\partial T/\partial y_s|_{T=T_{\max}} = 0$).

At last, for the W_{FE} coefficients (Fig. 7), the sensitivity at $x = 0$ mm is large. But, if we move away from this position, the sensitivity falls down $X_{W_{FE_{\max}}}(x = 0\text{ mm}) \approx -1000$ °C and $X_{W_{FE_{\max}}}(x = 2.5\text{ mm}) \approx 4$ °C. With the measurement errors equal to ±3%–4% of measured temperature, it seems to be difficult to estimate the W_{FE} value. Here again, we can note that this coefficient is proportional to $\partial T/\partial y_s$. So, this coefficient seems to be linearly dependent to the y_S coefficient.

With these three coefficients at $x = 2.5$ mm, we notice the coefficients tend to zero when we go away to the source position. So the estimations could be improved near this position with the measurements in $x = 2.5$ mm. Another approach to define the estimation domain is to compute the ratio between the normalized sensitivity coefficients.

4.4. Definition of the estimation domain

One way to study the dependence/no dependence between parameters is obtained by computing the ratio of the normalized sensitivity coefficients. In fact, if two parameters are dependent, the ratio is equal to a constant. Three ratios have been calculated for the three parameters. The evolution versus the longitudinal axis is reported in Figs. 8 and 9.

The ratio $X_{W_{FE}}/X_{P_W}$ (Fig. 8) shows that the two parameters are independent between $y = 0.01$ m and $y = 0.02$ m (around

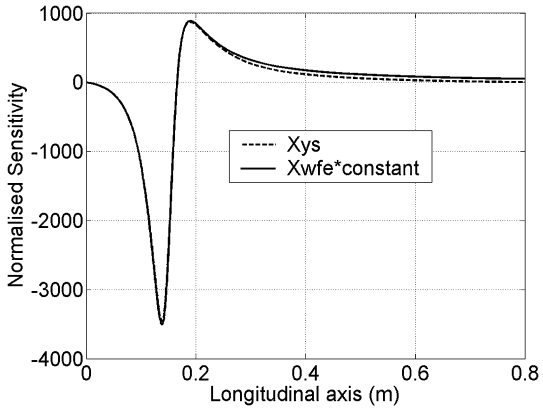

Fig. 9. Evolution of the Normalized sensitivities X_{y_S} and $X_{W_{FE}}$ at 2.5 mm from the source axis.

the source position $y_S = 0.015$). Out of this interval, the ratio is equal to a constant. The same observation is made for the ratio X_{y_S}/X_{P_W} (Fig. 8). The two parameters are independent in the same interval.

In Fig. 9, the two normalized sensitivity coefficient distributions X_{y_S} and $X_{W_{FE}}$ are plotted. The normalized sensitivity coefficients $X_{W_{FE}}$ has been multiplied by a coefficient defined by the maximum absolute value of X_{y_S} divided by the maximum value of $X_{W_{FE}}$. We can note that the two parameters are totally dependent along the longitudinal axis. Due to this behavior for these two parameters at $x = 2.5$ mm, simultaneous identification of y_S and W_{FE} by Levenberg–Marquardt is not possible.

In conclusion, the identifications seem to be possible in the domain around the source position for the couples (P_W, y_S) and (P_W, W_{FE}). The large magnitude of their sensitivity coefficients (except for W_{FE}) and their independence from each other allow a good estimation. The identification of W_{FE}, the "diameter of the beam welding", will not be enterprise due to the low sensitivity and it dependence with the source position y_S. In the next section, the Levenberg–Marquardt algorithm is presented and some numerical cases of the parameters estimation are shown.

5. Numerical applications: Estimation of the source parameters

In the previous chapter, estimation of "beam welding diameter" W_{FE} has appeared impossible. So, in the following, the parameter estimations have been done for two couples of two parameters: (P_W, y_S), (P_W, W_{FE}) (the third parameter W_{FE} or y_S respectively is assumed to be known). The goal of this preliminary study is to verify the feasibility of the estimation or the non-feasibility.

5.1. The Levenberg–Marquardt algorithm

For these works, the Levenberg–Marquardt algorithm is used [20]:

Assume that the temperature measurements Y_i are given at each abscissa $y_i, i = 1, \ldots, I$. We choose an initial set of parameters $P^0 = \{P_W^0, y_S^0\}, \{P_W^0, W_{FE}^0\}$ and an initial value for the damping parameter $\lambda^0 = 0.001$. The iteration number is initialized ($k = 0$). Then,

Step 1: Solve the direct problem with the available estimate P^k in order to obtain the temperature vector $T(P^k) = (T_1, T_2, \ldots, T_I)$.
Step 2: Compute $S(P^k)$ from Eq. (12).
Step 3: Compute the sensitivity matrix J^k defined by Eq. (14) and then the matrix $\Omega^k = I$, by using the current values of P^k.
Step 4: Calculate the new set of estimate P^{k+1} from Eq. (13):

Remark. Here, theoretical measurements with no noise are used, so $W = I$ (the identity matrix).

Step 5: Solve the direct problem with the new estimate P^{k+1} in order to find $T(P^{k+1})$. Then compute $S(P^{k+1})$, as defined in step 2.
Step 6: if $S(P^{k+1}) \geqslant S(P^k)$, replace λ^k by $\lambda^{k+1} = 10\lambda^k$ and return to step 4.
Step 7: if $S(P^{k+1}) \leqslant S(P^k)$, accept the new set of estimate P^{k+1} and replace λ^k by $\lambda^{k+1} = 0.1\lambda^k$. Check the stopping criteria. Stop the iterative procedure if it is satisfied; Otherwise, replace k by $k + 1$ and go to step 3.

Remark about the stopping criterion:

It exists three formulation for the stopping criteria [20], we have chosen the following stopping criterion.

This criterion consists on testing if the least square norm is sufficiently small: $S(P^{k+1}) \leqslant \varepsilon_{\text{stop}}$, which is expected to be in the neighborhood of the solution.

5.2. Study of the estimation feasibility

Several cases are investigated:

Case #1: Identification of the power P_W and the source position y_S.
Case #2: Estimation of the power P_W and Electron Beam (EB) parameter W_{FE} (with $W_{FE} = \sqrt{\phi_E/8}$).

The values $P_W^0 = 5000\ \text{W m}^{-1}$, $W_{FE}^0 \approx 0.00176$ ($\phi_E = 5$ mm) and $y_S^0 = 0.01$ m are used as initial guess for the each cases of the inverse heat transfer problem. The damping parameter λ^0 is set to 0.001. Moreover, the value of y_S and W_{FE} are constrained. First, the value of y_S is taken between $y_{\min} = 0.01$ and $y_{\max} = 0.02$ because the fused zone is lower to 0.01 m. On the electron beam diameter, we impose constraints: for the W_{FE} values less than 5e−5 ($\phi_E = 0.15$ mm), Femlab cannot solve efficiently the direct problem because the source is too focalized for the meshgrid. A superior limit is also taken to 10 mm because the experimental EB diameter ϕ_E is near to 1 mm.

Fig. 10 shows the decreases of the cost function. The threshold of 10^{-6} is reached for the cases #1 and #2 after 8–9 iterations.

For the case #1, the sensitivity coefficients of P_W and y_S are large and the good values are obtained easily. The two pa-

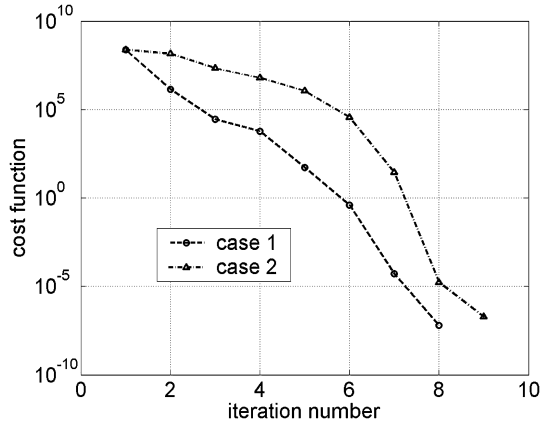

Fig. 10. Evolution of the cost function with the number of iteration.

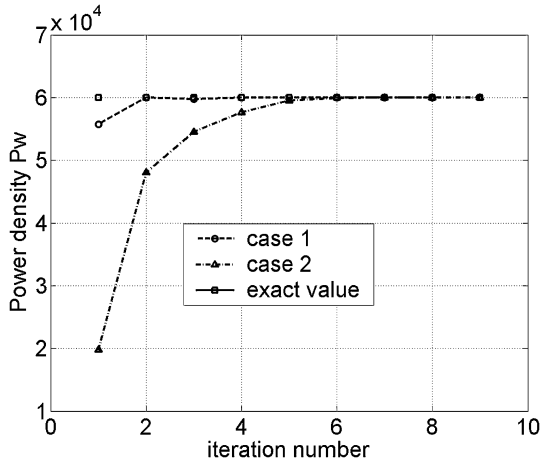

Fig. 11. Evolution of P_W parameter in function of iteration number.

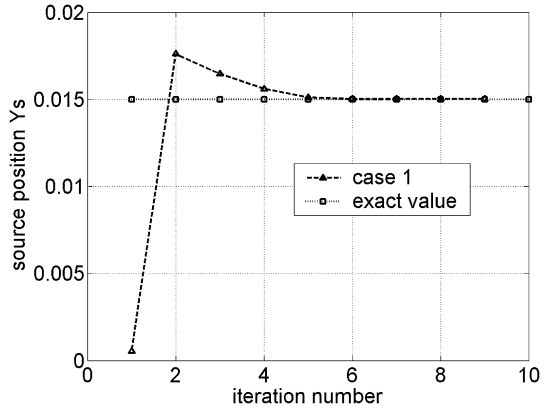

Fig. 12. Evolution of y_S parameter in function of iteration number.

rameters (Figs. 11 and 12) converge in the same time to the good values. After 8 iterations, the cost function is around 10^{-6} which corresponds to an average measurement error of 3.5×10^{-5} °C.

For case #2, the maximum of the P_W sensitivity coefficient is 300 times bigger than the one of the EB parameter W_{FE}. Nevertheless, the good values are reached after 2 iterations for P_W and 6 iterations for W_{FE} (Fig. 13). The cost function is around 10^{-6} for the iteration 8.

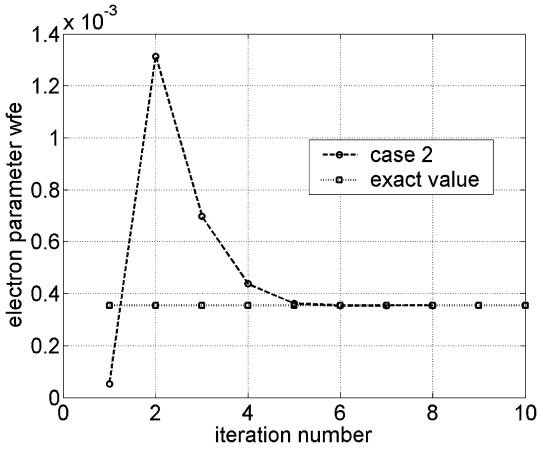

Fig. 13. Evolution of electron beam parameter in function of the number of iterations.

The two identification cases are possible in this paragraph: either the simultaneous identification of the power P_W and the source position y_S or the power P_W and the electron beam parameter W_{FE}. So, we shall work on the identification of power and the source position because of their high sensitivities contrarily to the electron beam parameter. The influence of parameter errors on the estimations are studied in the following paragraph.

5.3. *Influence of the parameter errors on the estimations*

Four cases are studied in this paragraph. Each cases consist in the resolution of the inverse heat transfer problem by using measurements with errors. These errors become from few origins: noise measurements due to the acquisition, error on the electron beam parameter choice and error on the sensor location. Generally, all these errors are present in the experimental measurements. Thus, the four studied cases are:

Case 3: Identification of P_W and y_S with the electron beam (EB) parameter value fix to $W_{FE} \sim 0.0007$ (or $\phi_E = 2$ mm) instead of $W_{FE} \sim 0.00035$ (or $\phi_E = 1$ mm) which has been used to obtain the exact data.

Case 4: P_W and y_S are estimated from exact measurements in $x = 2.4$ mm and estimated in $x = 2.5$ mm.

The case 5 consists in evaluating the influence of noise measurements on the parameter estimations. The noised temperatures are obtained by adding a standard noise deviation: $T_{\text{noised}} = T_{\text{exa}} + 0,04 \times \mu \times T_{\text{exa}}$ where μ is a random number between $[-1, 1]$.

Finally, case 6 studies the influence of these three mixed errors.

The results of the estimation procedure are summarized in Table 1. In the case 3, the cost function decreases to a lower value predicted for the threshold than the three others cases. The reached thresholds are predicted by calculating the quadratic sum of the difference between perturbed and exact temperatures:

$$S_{\text{Thres}} = [Y_i - T_i]^{\text{T}}[Y_i - T_i] = \sum_i (Y_i - T_i)^2 \tag{18}$$

Table 1
Final values of the four parameter estimations

	P_W [W m^{-1}]	y_S [m]	k	$S_{\text{Thres}}/S(P^k)$ estimated	Integral energy [W]
Good values	60000	0.015			94248
Case 3	59999.996	0.01509	8th	$3302/1.63\times10^{-6}$	94248
Case 4	60872.048	0.014954	6th	57110/57088.3	95618
Case 5	59748.78	0.014991	7th	487690/486007.7	93853
Case 6	60804.27	0.015003	6th	544480/521080.4	95511

where $Y_i = T_i$ (P_{Wexa}, y_{Sexa}, $W_{FE} = 1$ mm) is the exact data and $T_i = T$ (P_{Wexa}, y_{Sexa}, $W_{FE} = 2$ mm) (case 3), $T_i = T$ (P_{Wexa}, y_{Sexa}; $x = 2.4$ mm) (case 4), $T_i = T_{\text{noised}}$ (case 5) or $T_i = T_{\text{noised}}$ (P_{Wexa}, y_{Sexa}; $x = 2.4$ mm; $W_{FE} = 2$ mm) (case 6) are the perturbed data. The cost function for the cases 4, 5 and 6 have decreased rapidly to their respective predicted threshold and stabilizes (less than 8th iterations, Table 1).

The energy integral is well identified in each cases (Table 1). It is defined so:

$$I_{\text{Energy}} = \iint S(x,y)\,\mathrm{d}x\,\mathrm{d}y = \iint \left(\frac{P_W}{W_{FE}^2}\exp\left[-\frac{x^2+(y-y_S)^2}{W_{FE}^2}\right]\right)\mathrm{d}x\,\mathrm{d}y \qquad (19)$$

The most accurate is achieved with the error on EB parameter W_{FE} (case 3). This error does not exceed 1.5% of the good value.

The power P_W and the source position y_S are well estimated for the four cases. The power P_W is the less accurate. The power density and the source position are very sensitive to the sensor position. An error of 1 mm for the source position gives errors of 1.5% for the power and 0.2% for the source position y_S. The power is so overestimated and the source position is located forward to the good value. In the case 5, noised measurements lead to underestimated power.

Finally, the study of these four cases shows that the estimation of power and source position is possible with a good accuracy. Sensor location errors, measurement errors or electron beam diameter errors do not prevent the estimation of the P_W and y_S parameters. That shows the robustness of the Levenberg–Marquardt method.

5.4. Conclusion

In this chapter, numerical results have been presented. We have seen that the identification of power and the source position is realizable whereas the identification of the electron beam diameter is impossible due to its low sensitivity and its dependence with the source position parameter. In each investigated cases: electron beam diameter errors, measurement errors or sensor position errors do not prevent a good estimation. To perform the identification from experimental measurement, we must choose a value for the electron beam diameter. This choice can be done after having solved the inverse heat transfer problem with different value of W_{FE}. In the last chapter, experimental measurements are used for the parameter identifications.

Table 2
The temperature measurement positions

	x (m)	z (m)
Measure $R26$	0.0023	0.0098
Measure $R04$	0.0023	0.0223
Measure $R06$	0.0018	0.0348
Measure $R20$	0.0023	0.047
Measure $R19$	0.002	0.0523
Measure $R16$	0.0011	0.0673

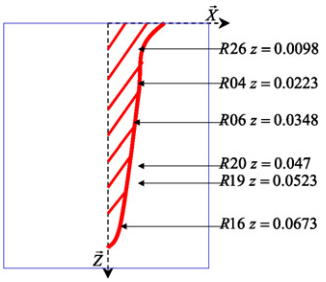

6. Experimental identification of the source

The measured temperatures used in this chapter come from an experiment realized with the Electron Beam welding process of the DCN-Propulsion Indret, France (44). This experiment is presented in the thesis of Jialin Guo [21]. The experimental parameters are: The tension $U = 60$ kV, the current $I_b = 0.29$ A, the velocity $V = 2.5$ mm s^{-1}. In this experiment, the measurements are realized in the Heat Affected Zone with 93 type K thermocouples. Here, we use only 6 of them for the validation of the estimation method. Table 2 shows the thermocouple positions.

The aim of this chapter is the identification of the experimental value of P_W and y_S. The electron beam parameter is chosen to $W_{FE} \approx 0.000353$ ($\phi_E = 1$ mm). The initial set of the parameters is again the one used for the previous numerical applications: $P_W = 5000$ W m^{-1}, $y_S = 0.01$ m.

6.1. Results of the parameter estimation

The inverse problem is solved until the cost function is stabilized or the criterion $\|P^{k+1} - P^k\|/\|P^k\| \leqslant \varepsilon_{\text{stop}}$ is validated ($\varepsilon_{\text{stop}} = 1\%$).

Fig. 14 shows the evolution of the cost function for an electron beam parameter $W_{FE} \approx 0.000353$ ($\phi_E = 1$ mm). Table 3 gives the results of the P_W and y_S estimations. For the depths $z = \{2.23\text{ cm}; 3.48\text{ cm}; 4.7\text{ cm}; 5.23\text{ cm}\}$ the cost function stabilizes about 10^6. All power P_W and source position y_S val-

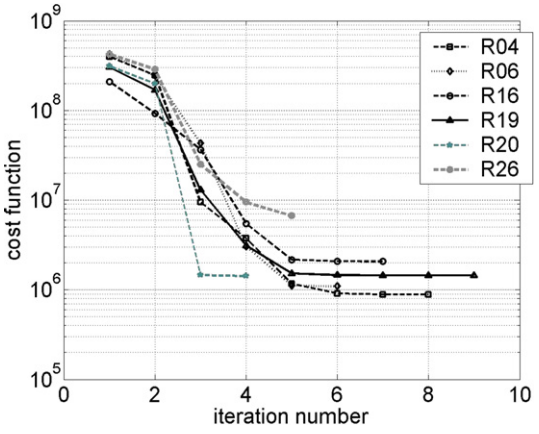

Fig. 14. Evolution of the cost function for the different temperature measurements.

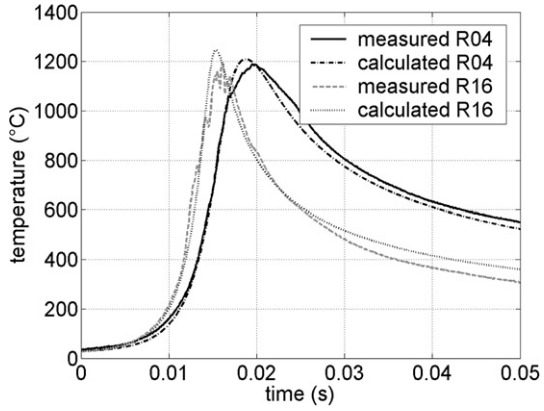

Fig. 15. Comparison between measured and calculated temperatures (R16 is located at $x = 1.1$ mm and $z = 67.3$ mm and R04 is situated at $x = 2.3$ mm and $z = 22.3$ mm).

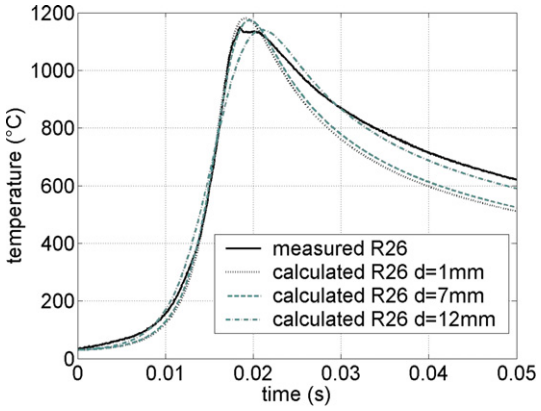

Fig. 16. Comparison between measured and calculated temperatures at ($x = 2.3$ mm; $z = 9.8$ mm).

Table 3
Estimated values for the parameters with $\phi_E = 1$ mm

	P_W [W m^{-1}]	y_S [m]
Measure $R26$	56381.3	0.017
Measure $R04$	58270.6	0.0166
Measure $R06$	57938.2	0.0164
Measure $R20$	52264.3	0.0167
Measure $R19$	51051.7	0.016
Measure $R16$	39943.9	0.014

Table 4
Estimated values for the temperature measurement $R26$ with different electron beam diameter

	P_W	y_S	$S(P^k)$ final	ϕ_E
Measure $R26$	56381.3	0.017	6.69×10^6	1 mm
Measure $R26$	58391.4	0.0176	3.53×10^6	7 mm
Measure $R26$	66680.5	0.0179	1.19×10^6	12 mm

ues are quite the same: 52000 W m^{-1} ($z \sim 5$ cm) $\leqslant P_W \leqslant$ 58000 W m^{-1} ($z \geqslant 4$ cm) and $y_S \approx 0.0165$ m. Fig. 15 shows the comparison between the experimental and calculated temperatures.

Excepted for the maxima of the temperature, we find a good agreement between the measured and calculated temperatures especially during the heating and cooling phases of the thermal cycles. Consequently in this central zone of the welding strand, the 2D quasi-steady model (x, y) and the Gaussian source modelise quite well the heat transfer.

On the other hand, at the foot ($z \sim 67.3$ mm) and the head of the weld strand ($z \sim 9.8$ mm), we have difficulties to fit the thermal cycle. At the foot of the weld strand, the Fig. 15 shows a good agreement between measured and calculated kinetics until $y \leqslant 25$ mm. Beyond we have a cooling temperature measured faster than calculated temperature probably due to the matter below the weld strand which pumps the heat. The bidimensional model is not valid. The estimated power P_W seems to be good and is less than the values estimated in the middle of the weld strand. The estimated source position y_S at the foot of the weld strand let thinking that the electron beam is sloped forward. This analysis is unrealistic. As a matter of fact the delay of the source in the central weld strand is probably due to convective movements of the liquid matter which throw again the energy at the back of the electron beam. It is observed at the head of the weld strand where the convective movements are more important. A throwing up of fused matter at the back brings heat to the surface. This heat is dissipated either by heat radiation transfer towards the exterior surroundings or by conduction. That is why the bidimensional quasi-steady model cannot represent correctly the phenomena. It is shown in Fig. 16 where we compare measured and calculated kinetics for measurements at the head of the weld strand. Due to the convective energy contribution at the back of the electron beam the experimental kinetic is hotter at cooling. In reality, near to the surface, we should modelise the source with a decentred ellipsoid Gaussian instead of a circular Gaussian. However, we tried few values of electron beam diameter to validate our Gaussian model: $W_{FE} = \{3.53 \times 10^{-4};\ 2.32 \times 10^{-3};\ 4.2 \times 10^{-3}\}$ ($\phi_E = \{1\text{ mm}, 7\text{ mm}, 12\text{ mm}\}$ respectively). Table 4 shows that the cost function decreases when the electron beam diameter increases. At the same time, the source position moves back and the power increases. This result confirms the hypothesis of the rejected energy at the back of the electron beam. Nevertheless this increase of the diameter is limit: in Fig. 16 the temperature calculated for $\phi_E = 12$ mm rises faster than the measured temperatures. Large diameters produce a premature augmentation of the temperature at the front of the electron beam.

6.2. Conclusions

The identification results show that the power and the source position remain constant in the middle of the weld strand. It could signify that the assumptions of our modeling are sufficient in this part of the weld strand. For the top and the bottom of the weld strand, it is quite different. At the top of the weld strand, we did not happen to modelise the cooling phase of the temperature evolution with the longitudinal axis, a contrario, at the foot of the weld strand, we overestimate the cooling phase. At the top, we neglect the convective movement of the liquid metal that can be the cause of the underestimation of the cooling phase whereas at the bottom, the mass of metal under the weld strand absorbs the heat that refreshes more rapidly. Typically,

value of 52–58 kW m^{-1} for the power and a source position of 0.0165 m are estimated in the middle of the weld strand. The power value is near than the one proposed from experimental data.

7. Conclusions

In this work, we have presented the electron beam welding process. The thermo-metallurgical modeling of the process needs the knowledge of heat source generated by the electron beam. After having presented the complete modeling of the process, we have assumed that the parameters are no temperature dependent. In fact, this assumption is done for the resolution of the inverse heat transfer problem of identification of the heat source. The method used to solve the inverse problem has been developed, first, by Levenberg then modified by Marquardt. This method needs a sensitivity analysis before beginning the resolution of the inverse problem. The sensitivity analysis has shown that temperature measurements located at 2.5 mm from the source line does not allow the identification of the electron beam parameter W_{FE}. So the theoretical identifications have consisted in the estimation of the power P_W and the source position y_S.

For the experimental estimations, we show that the 2D quasi-steady state model and the Gaussian source represent well the phenomena in the middle of the weld strand. On the other hand, near the head of the weld strand, the phenomena are more complicated to modelise. We should take a tridimensional model with an ellipsoidal source. Moreover, a 3D non-linear thermometallurgical model should be developed. The difficulty is to define correctly the formulation of the source.

This study has shown the feasibility of use of the Levenberg–Marquardt method for the identification of the heat source.

References

[1] J. Guo, P. Le Masson, E. Artioukhine, T. Loulou, P. Rogeon, M. Carin, M. Dumons, J. Costa, Estimation of a source term in a two dimensional heat transfer problem: Application to an electron beam welding, in: 4th Int. Conf. Inverse Problems, Russia, 2003.

[2] J.V. Beck, B. Blackwell, C.R.St. Clair, Inverse Heat Conduction: Ill Posed Problems, Wiley Interscience, New York, 1985.

[3] O.M. Alifanov, E. Artyukhin, A. Rumyantsev, Extreme Methods for Solving Ill-Posed Problems with Applications to Inverse Heat Transfer Problems, Begell House, New York, 1995.

[4] Y. Jarny, N. Ozisik, J.P. Bardon, A general optimization method using adjoint equation for solving multidimensional inverse heat conduction, Int. J. Heat Mass Transfer 62 (1991) 2911–2919.

[5] A.J. Silva Neto, et al., Two dimensional inverse heat conduction problem of estimating the time-varying strength of a line source, J. Appl. Phys. 171 (1992) 5357–5362.

[6] C. Le Niliot, The boundary element method for the time varying strength estimation of point heat sources: Application to a two-dimensional diffusion system, Numer. Heat Transfer B 33 (1998) 301–321.

[7] C. Le Niliot, et al., Infrared thermography applied to the resolution of inverse heat conduction problems: Recovery of heat line sources and boundary conditions, Rev. Gen. Therm. 37 (1998) 629–643.

[8] S. Peneau, et al., Front motion and convective heat flux determination in a phase change process, Inverse Problem Engrg. 4 (1996) 53–91.

[9] R. Keanini, et al., Inverse finite element reduced mesh method for predicting multidimensional phase change boundaries and nonlinear solid face heat transfer, Int. J. Heat Mass Transfer 39 (1996) 1039–1049.

[10] Y.F. Hsu, et al., An inverse finite element method for the analysis of stationary arc welding processes, J. Heat Transfer 108 (1986) 734–741.

[11] Y. Ruan, et al., An inverse finite element technique to determine the change of phase interface location in two dimensional melting problems, Commun. Appl. Numer. Methods 7 (1991) 325–338.

[12] N. Zabaras, Adjoint methods for inverse free convection problems with application to solidification processes, in: Computational Methods for Optimal Design and Control, Birkhäuser, Basel, 1998, pp. 391–426.

[13] V. Karkhin, et al., Solution of inverse heat conduction problem for determining heat input, weld shape, and grain structure during laser welding, Sci. Tech. Welding Jioning 7 (4) (2002) 224–231.

[14] K. Levenberg, A method for the solution of certain non linear problems in least squares, Quart. Appl. Math. 2 (1944) 4164–4168.

[15] D.W. Marquardt, An algorithm for least squares estimation of non linear parameters, J. Soc. Ind. Appl. Math. 11 (1963) 431–441.

[16] M. Costantini, Simulation numérique du soudage par faisceau d'électrons, contribution au développement d'un modèle prédictif de l'apport d'énergie, Thèse de l'université Paris 6, 1995.

[17] M. Carin, et al., Experimental validation of a predictive model for numerical simulation of thermo-metallurgical phenomena during electron beam welding, in: 2nd Int. Conf. on Thermal Process Modelling and Computer Simulation, France, 2003.

[18] P. Rogeon, et al., Numerical simulation of electron beam welding of metals: sensitivity study of a predictive model, in: H. Cerjak, H.K.D.H. Bhadeshia (Eds.), Mathematical Modelling of weld Phenomena 5, Institute of Materials, 2001, pp. 913–943.

[19] Handbook of Sysweld, Systus International, 1994.

[20] M.N. Ozisik, H.R.B. Orlande, Inverse Heat Transfer: Fundamentals and Applications, Taylor and Francis, New York, 2000.

[21] J. Guo, Estimation de la distribution énergétique induite par un faisceau d'électrons dans un matériau métallique – Application au cas du soudage d'un acier, Thèse de l'université de Bretagne Sud, 2005.